Int J Adv Manuf Technol (2014) 72:1677–1686
DOI 10.1007/s00170-014-5760-4

ORIGINAL ARTICLE

A new CAD/CAM/CAE integration approach to predicting tool deflection of end mills

Liming Wang · Zezhong Chevy Chen

Received: 19 September 2013 / Accepted: 6 March 2014 / Published online: 30 March 2014

Abstract Tool deflection of end mills caused by cutting forces has a great effect on the machining quality and efficiency. Cylindrical cantilever beam model with 80 % of tool radius is generally used to predict the tool deflection roughly. But that ignored the complex geometrical structure of end mills, which is manufactured with a set of grinding operations. In this study, the geometrical model of end mill is developed based on the CAD/CAM integration via modeling its grinding processes. Using the developed CAD model, the cutting coefficients and distributed cutting forces along the tool axis are obtained via finite element analysis of cutting simulation. Besides, the moment of inertia along the tool axis is also precisely measured based on the CAD model. Finally, with the measured inertia and distributed cutting forces, the tool defection can be predicted accurately with the unit loading algorithm for the cantilever beam. This study provides an accurate approach to predicting tool deflection of end mills based on the CAD/CAM/CAE integration.

Keywords Tool deflection · End mill · CAD/CAM/CAE integration

1 Introduction

Milling is used widely in manufacturing industry due to its large material removal rate and high surface quality. Tool deflection caused by cutting forces is a common problem in manufacturing processes, which would greatly affect the machining efficiency and quality [1–6]. As the most flexible part in machine structure, end mills generally contribute the most to the tool deflection in the milling processes [7]. In practice, trial-and-error experiments are often applied to select the proper end mills and machining parameters, which is quite expensive and time consuming [8], especially when high precise machining is required.

In previous researches [1, 9–13], the tool deflection is predicted through modeling the end mill as a cantilever cylindrical beam rigidly supported by the tool holder, subject to a concentrated force at the end or evenly distributed loads along its axis. In Kops' research [9], the cylindrical diameter was first proposed as 80 % of the tool's diameter. And also, the surface quality is investigated via calculating the tool deflection base on the cylindrical model [1, 10]. However, as shown in Fig. 1, the end mill is formed with complex helix flutes. The flute space will greatly affect the static and dynamic properties of end mills [14]. What is more, the cutting forces are unevenly distributed along the cutting edges and varying with cutting rotation in the milling processes. Therefore, those assumptions of the cylindrical models ignore the varies of flute shape, such as various core radius and flute length, and thus, would introduce errors for the predicted results, especially for some slender tools with long flutes. To improve the machining efficiency and accuracy, it is in high demand that a new and accurate approach to determining the tool deflection in milling processes.

Regardless of the above algorithms, developing the geometrical model of end mill and predicting the unevenly distributed milling forces along the tool axis are two major problems to improve the accuracy of predicting the tool's deflection. In this paper, an accurate approach is developed to predict the tool deflection considering the geometrical model of end mill and the distribution of cutting forces based on the CAD/CAM/CAE integration. First, a parametric CAD model of end mill, including the helix flutes and cutting edges, was developed based on CAD/CAM integration of end mills

L. Wang (✉) · Z. C. Chen
Department of Mechanical and Industrial Engineering, Concordia University, Montreal, Quebec, Canada H3G 1M8
e-mail: walimine@gmail.com

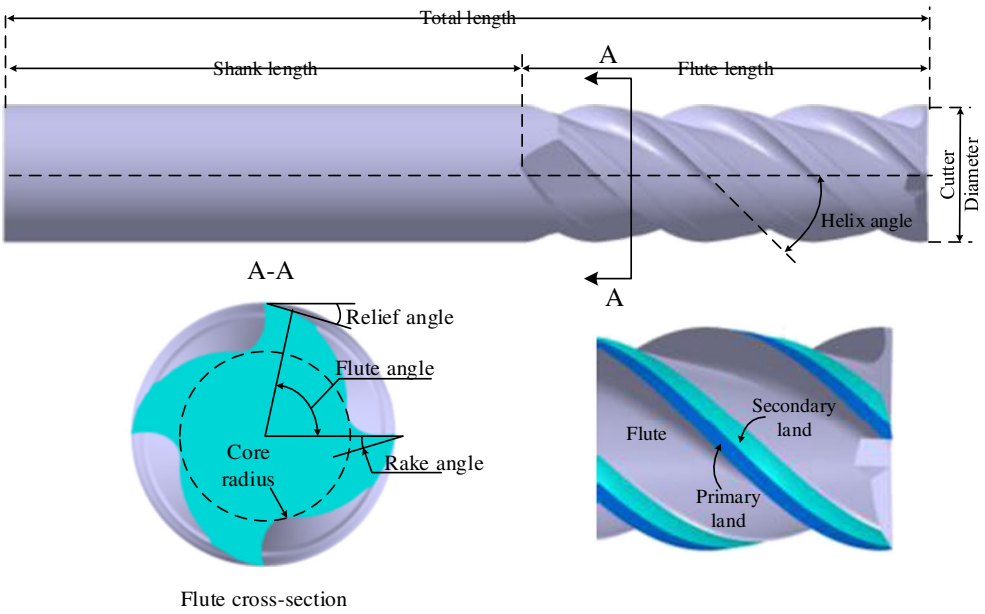

Fig. 1 Illustration of end mill geometry

via modeling the kinematics of the grinding processes. Besides, the cutting simulation was conducted through finite element analysis (FEA) of milling processes to evaluate cutting coefficients and calculate distributed cutting forces. Finally, the tool deflection is obtained and validated using the unit loading algorithm with the predicted distributed cutting forces.

2 CAD/CAM integration for modeling end mill

A five or four-axis CNC grinding machine is generally employed to construct the grinding processes of end mills, and the NC programming is generated automatically with the commercial CAM software in industry [15]. The shape of end mill is formed based on the kinematics between the moving grinding wheel and cutter at each operation [16–18]. It is difficult to model the exact three-dimensional shape of end mills because a certain part of the shape is not determined until the actual machining operation [19]. Therefore, the geometrical model of end mill can only be developed via simulating and modeling its grinding processes. Hereto, two major grinding processes are introduced in this work including flute-grinding and cutting-edge-grinding.

In this paper, a three-layer framework of CAD/CAM integration system is proposed illustrated in Fig. 2. The first layer is the design parameters, including the basic information of the end mills, such as tool radius, rake angles, relief angle, etc., whose values should be provided by the designers. The second layer is the CAM system which is aimed to program the planning of grinding processes to satisfy the requirement of the design parameters provided by the first layer. In the second layer, the main task is to determine the proper geometry of grinding wheel and develop the kinematics of grinding processes. The third layer is the CAD system, which is used to generate the CAD model of end mill through calculation of the swept volume of the grinding wheel at different position and orientation provided by the second layer. Finally, the

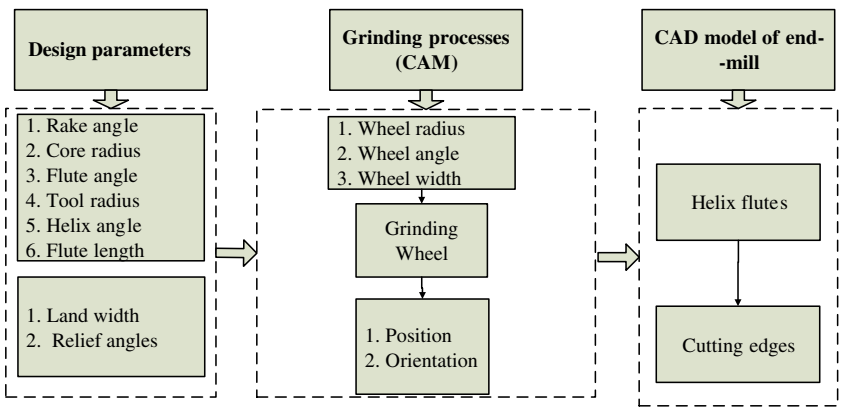

Fig. 2 CAD/CAM integration for end mill

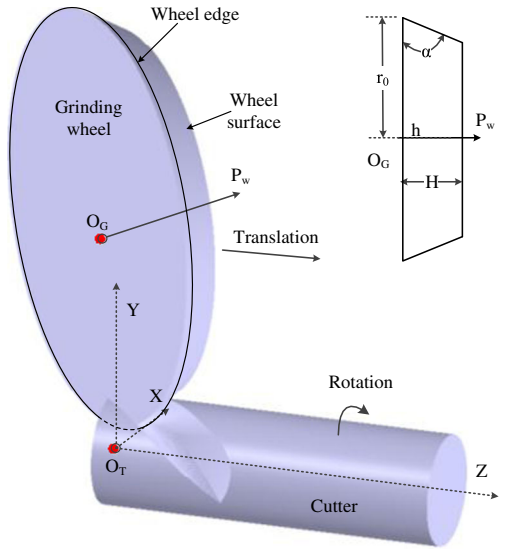

Fig. 3 Illustration of the flute-grinding process

integration of CAD/CAM for end mills is accomplished through the data transmitted layer by layer.

2.1 Flute modeling

The helix flute is generated with intersection between the grinding wheel and the cutter with a helix motion. The working area of grinding wheel occurs at the wheel edge and wheel surface shown in Fig. 3. A parametric grinding wheel is illustrated in Fig. 3 with wheel angle α, wheel width H, and wheel radius r_0, and the representation is given in Eq. (1):

$$\mathbf{r}_w = \begin{bmatrix} r \cdot cos\theta \\ r \cdot sin\theta \\ h \end{bmatrix}, \tag{1}$$

where, $r = r_0 - h \cdot \cot\alpha$ and $h \in [0 \quad H]$.

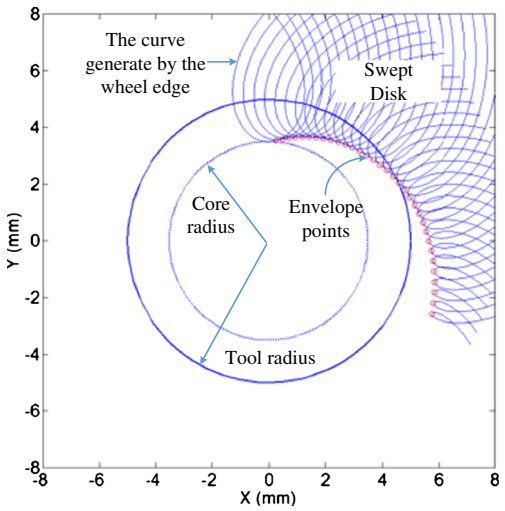

Fig. 4 Simulation of the flute shape in the cross-section

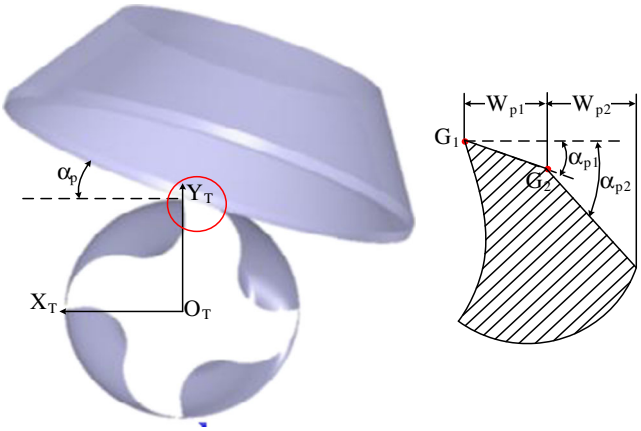

Fig. 5 Illustration of the cutting-edge-grinding process

In order to model the flute-grinding process, a right-hand tool coordinate system is developed, of which the origin $\mathbf{O_T}$ is located at the center of left end of the cutter. Initially, the grinding wheel is set up with a specific position $\mathbf{O_G}$ and orientation $\mathbf{P_w}$. As described in Fig. 3, $\mathbf{O_G}$ is the center point of the grind wheel at the larger end and $\mathbf{P_w}$ is unit vector along wheel axis. The setup operation can be expressed with a homogeneous matrix shown in Eq. (2):

$$\mathbf{M}_1 = \begin{bmatrix} \cos\beta & 0 & \sin\beta & dx \\ 0 & 1 & 0 & dy \\ -sin\beta & 0 & \cos\beta & dz \\ 0 & 0 & 0 & 1 \end{bmatrix}, \tag{2}$$

where, β is the angle between $\mathbf{P_w}$ and Z axis, $[dx\ dy\ dz]$ is the coordinate value of $\mathbf{O_G}$ in the tool coordinate system.

After that, the wheel will moving with a translation along the tool axis and the cutter rotate with a specific angular velocity to generate the helix flute surface. This process can

Table 1 Key parameters of the end-mill (length unit: mm, angle unit: deg.)

Tool parameters	Value	Description
Total length	60.00	
Flute length	18.00	
Tool diameter	6.00	
Helix angle	45.0	
Rake angle	4.9	Radial direction
Core diameter	3.60	
1st Relief angle	9.0	
2nd Relief angle	18.0	
1st Land width	0.83	Normal to the cutting edges
2nd Land width	1.25	Normal to the cutting edges

Table 2 Machining parameters for flute-grinding processes

dx (mm)	*dy* (mm)	*dz* (mm)	β (deg.)	r_0 (mm)	α (deg.)	H (mm)
−33.399	70.592	−8.000	47.18	75.000	90.00	1.924

be represented in the tool coordinate system using another homogeneous matrix in Eq. (3):

$$\mathbf{M}_2 = \begin{bmatrix} \cos\omega & -\sin\omega & 0 & 0 \\ \sin\omega & \cos\omega & 0 & 0 \\ 0 & 0 & 1 & \frac{\omega \cdot r_1}{\tan\delta} \\ 0 & 0 & 0 & 1 \end{bmatrix}, \tag{3}$$

where, ω is the rotation angle, δ is the helix angle of cutter, and r_1 is the tool radius.

Integrating Eqs. (1) to (3), the representation of the flute-grinding processes at any instant is obtained in the tool coordinate system shown in Eq. (4):

$$\mathbf{r}_T = \begin{bmatrix} (r{\cdot}cos\theta{\cdot}\cos\beta + h{\cdot}\sin\beta + dx){\cdot}cos\omega - (rsin\theta + dy){\cdot}sin\omega \\ (r{\cdot}cos\theta{\cdot}\cos\beta + h{\cdot}\sin\beta + dx){\cdot}sin\omega + (rsin\theta + dy){\cdot}cos\omega \\ \frac{\omega \cdot r_1}{\tan\delta} - r{\cdot}cos\theta{\cdot}\sin\beta + h{\cdot}\cos\beta + dz \end{bmatrix}. \tag{4}$$

In general, the flute shape is investigated in the cross-section (*XY* plane) that is setting $\frac{\omega \cdot r_1}{\tan\delta} - r{\cdot}\cos\theta{\cdot}\sin\beta + h{\cdot}\cos\beta + dz = 0$. We will get the representation of flute shape in the cross-section shown Eq. (5):

$$\mathbf{r}_c(\theta, h) = \begin{bmatrix} (r{\cdot}cos\theta{\cdot}\cos\beta + h{\cdot}\sin\beta + dx){\cdot}cos\omega - (rsin\theta + dy){\cdot}sin\omega \\ (r{\cdot}cos\theta{\cdot}\cos\beta + h{\cdot}\sin\beta + dx){\cdot}sin\omega + (rsin\theta + dy){\cdot}cos\omega \end{bmatrix}, \tag{5}$$

where, $\omega = \frac{(r{\cdot}\cos\theta{\cdot}\sin\beta - h{\cdot}\cos\beta - dz){\cdot}\tan\delta}{r_1}$.

As shown in Fig. 4, a Matlab program is developed to simulate the above processes. It is observed that the flute shape consist of two connected curves: (a) the first curve generated by the wheel edge and (b) the second curve generated by the envelope of wheel surface. For the first curves, it can be obtained by setting h=0 in Eq. (5). For the enveloping curve, the wheel surface is discritized into sets of finite disks and each disk is swept and intersected with the cross-section. The enveloping curve is deduced from a

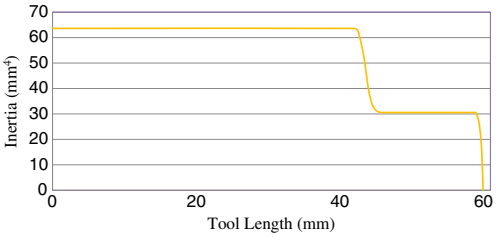

Fig. 7 Moment of inertia I_y along the tool axis

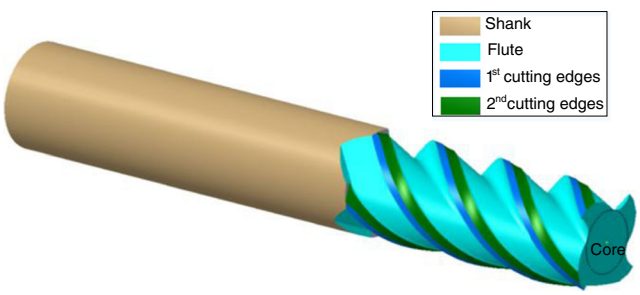

Fig. 6 CAD model of the end-mill

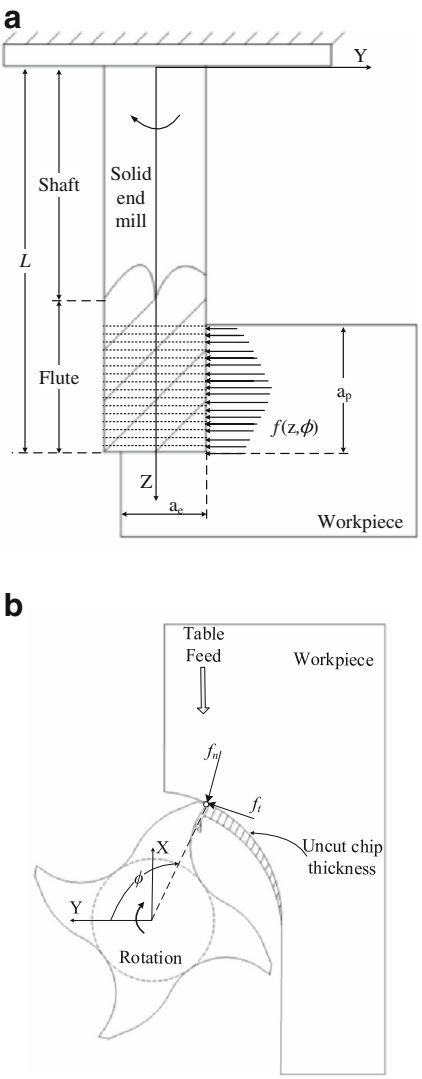

Fig. 8 Cutting forces in the milling processes

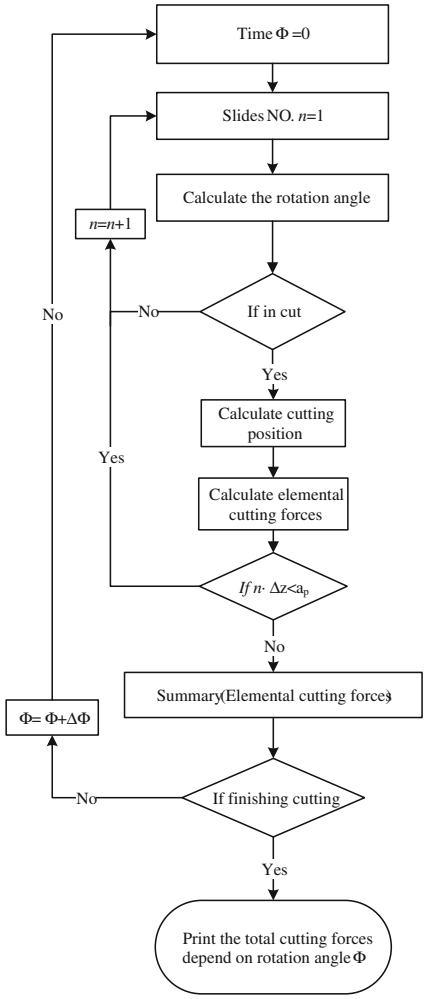

Fig. 9 Cutting forces prediction flowchart

family of swept disk based on the envelope theorem in Eq. (6) described in Fig. 4:

$$\frac{\partial \mathbf{r}_c}{\partial \theta} \times \frac{\partial \mathbf{r}_c}{\partial h} = 0. \tag{6}$$

2.2 Cutting-edge modeling

Basically, for each flute, there are two cutting edges, called the first cutting edge and the second cutting edge, which are defined by the corresponding relief angles (α_{p1}, α_{p2}) and land widths (W_{p1}, W_{p2}) shown in Fig. 5; the cutting edges are ground by the wheel edge. Initially, the grinding wheel is configured with an angle α_p and then grinding via helix motion which is result from the translation of the grinding wheel and the rotation of the cutter. In the cutting-edge-grinding process, the configuration angle α_p is determined by corresponding relief angles: α_{p1}, α_{p2}. Similarly with the flute-grinding, the helix motion is governed by the transformation matrix in Eq. (3). In this process, the relief angles and land widths are obtained. The mathematical expression of the first and second land surfaces are derived using a general form of equation shown Eq. (7).

$$\mathbf{r}_{land}(\mu,\omega) = \begin{bmatrix} W_p \cdot \mu \cdot \cos\omega - \left(r_p - W_p \cdot \tan\alpha_p \cdot \mu\right) \cdot \sin\omega \\ W_p \cdot \mu \cdot \sin\omega + \left(r_p - W_p \cdot \tan\alpha_p \cdot \mu\right) \cdot \cos\omega \\ \dfrac{\omega \cdot r_1}{\tan\delta} \end{bmatrix}, \tag{7}$$

where $\mu \in [0,1]$, α_p is the relief angle, W_p is the land width, and r_p is the radius from the tool origin O_T to the grinding

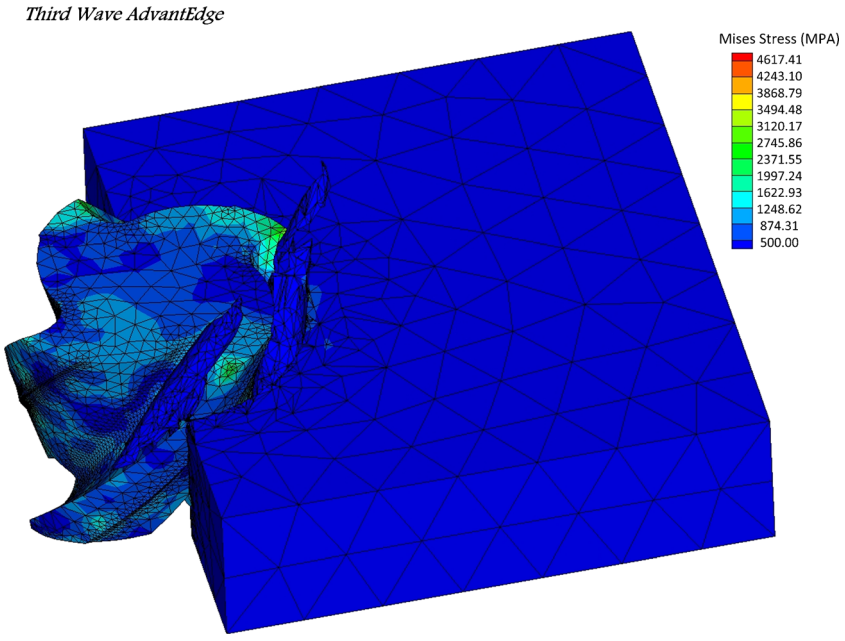

Fig. 10 Full immersion cutting simulation with *AdvantEdge*

Table 3 Material properties of the end-mill and work-piece

Material properties	End mill	Work-piece
Material	Tungsten carbide	AISI4140 Alloy steel
Modulus of elasticity	690 Gpa	200 GPa
Poisson's ratio	0.24	0.3
Density	14,800 kg/m^3	7,850 kg/m^3
Hardness, Brinell	2,570 N/mm^2	1,049 N/mm^2
Yield strength	–	821 MPa
Ultimate tensile strength	–	1,073 MPa

point G_1 or G_2 corresponding to the first and second land surface described in the break view in Fig. 5.

2.3 Validation of the proposed CAD model

To demonstrate the validity of proposed CAD/CAM integration approach, the end mill model was simulated with the *volume-sweep* function in software CATIA. In this example, a four-flute end mill is designed and the corresponding parameters are specified in Table 1. In order to guarantee the design parameters, the CAM processes were developed to machine the flute. In the flute-grinding simulation, the grinding wheel dimension r_0, α, H and its position [*dx dy dz*], setting-up angle β are illustrated in Table 2. The first and second relief angles are 9° and 18°, respectively, which are used to model the cutting edges. Finally, the solid CAD model is obtained from the grinding processes shown in Fig. 6. Besides, the moment of inertias along the tool axis is investigated from the developed CAD model with CATIA *measure* function shown in Fig. 7, which will be used in the following tool deflection prediction.

3 Cutting forces prediction

The cutting forces are generated in the milling processes while the rotating cutter removing the material, and the cutting

Table 4 Machining parameters and average cutting forces with *AdvantEdge*

No.	Cutting speed (m/min)	Feed rate *c* (mm/tooth)	Axial cutting depth a_p (mm)	$\overline{F_x}$ (*N*)	$\overline{F_y}$ (*N*)
1	160	0.03	3.00	−454.4	373.9
2	160	0.06	3.00	−732.3	471.7
3	160	0.10	3.00	−1094.7	505.4
4	160	0.12	3.00	−1271.1	557.9
5	160	0.15	3.00	−1519.9	606.0

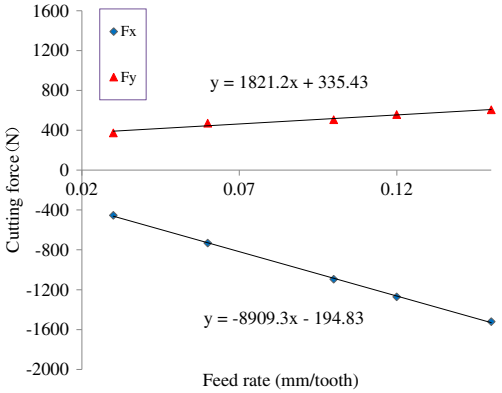

Fig. 11 Cutting forces measured for AISI4140

forces play an important role in the tool deformation, surface finish, tool wear, etc. Generally, the cutting forces are regarded as a linear function with respect to the feed rate and uncut chip thickness using cutting coefficients [2, 5]. In the milling processes, the cutting forces are distributed along the cutting edges with varying magnitudes and directions. In order to predict the distribution of the cutting forces, the end mill is divided into finite segments along the tool axis shown in Fig. 8a. For each segment, the elemental cutting forces are resolved into two direction and calculated by Eq. (8). The total cutting forces could be obtained by summing up all the elemental forces.

$$\begin{bmatrix} f_x \\ f_y \end{bmatrix} = \sum_{j=1}^{N} \begin{bmatrix} -\cos\phi & -\sin\phi \\ \sin\phi & -\cos\phi \end{bmatrix} \begin{bmatrix} K_{tc}h + K_{te} \\ K_{rc}h + K_{re} \end{bmatrix} \cdot \Delta z, \tag{8}$$

where, Δz is the discrete cutting depth along the tool axis; N is the tooth number; and K_{tc}, K_{te}, K_{rc}, and K_{re} are called cutting coefficients which are related to the tool geometry and machined material; h is the uncut chip thickness expressed in Eq. (9).

$$h = \begin{cases} c \cdot \sin\phi, & \phi_{entry} \le \phi \le \phi_{exit} \\ 0, & others \end{cases} \tag{9}$$

where, c is the feed rate per tooth; φ is the immersion angle shown in Fig. 8b; and φ_{entry}, φ_{exit} are the entry and exit angles.

Table 5 Cutting coefficients of AISI4140

Cutting coefficient	Value (MPa)
K_{tc}	607.1
K_{te}	87.8
K_{rc}	2,969.8
K_{re}	51.0

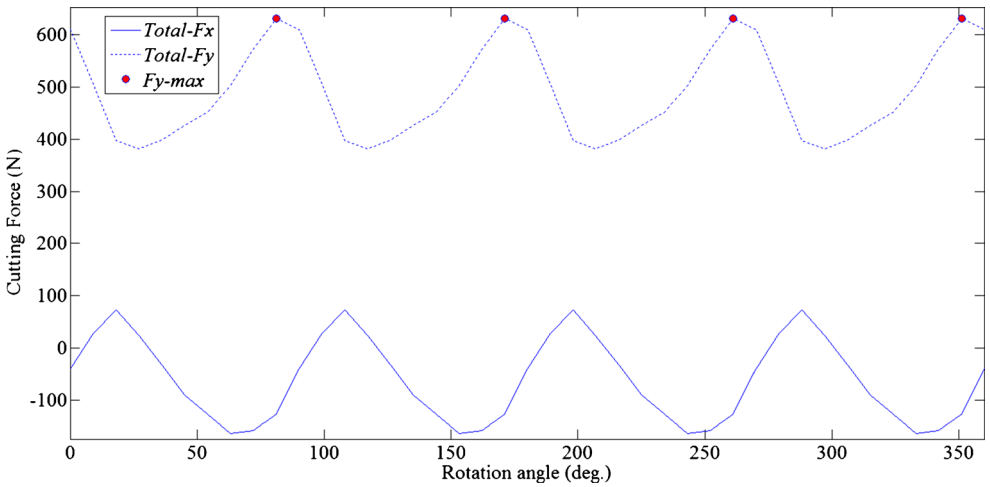

Fig. 12 Predicted milling forces for AISI4140

Besides, the position where the corresponding elemental cutting forces are applied is also represented in the coordinate system of Fig. 8 with the following matrix:

$$\begin{bmatrix} x \\ y \\ z \end{bmatrix} = \begin{bmatrix} r_1 \cdot \sin\phi \\ r_1 \cdot \cos\phi \\ L - n \cdot \Delta z \end{bmatrix}, \quad (10)$$

where, L is the suspended tool length and n is the segment sequence number.

In summary, as shown in the flow chart Fig. 9, the milling process is discretized in two aspects: in the time domain, it is examined angle by angle through discretizing the rotating immersion angle; in the space domain, it is divided along the tool axis and the elemental cutting forces are calculated based the above equations slides by slides. Finally, a Matlab program is developed to simulate the milling process. In the program, not only that the total cutting forces are obtained, but also the distributing elemental cutting forces are recorded.

AISI4140 alloy steel is a typical high strength material applied widely in industry, such as gear, automotive connecting rod, etc. Due to its high hardness, larger cutting forces are always produced and cause corresponding larger tool deflection. In workshop, the lower cutting depth and short tools are generally recommended to get higher machining accuracy [13]. But that would cost the machining efficiency to some extent. In this research, AISI4140 is used as the experimental material to predict the cutting forces and deflection in milling process.

As described in Eq. (8), the cutting forces are linear function of four cutting coefficients which are generally determined experimentally under various cutting condition. In this research, in order to get the cutting coefficients integrating with the developed end mill model, the full immersion milling

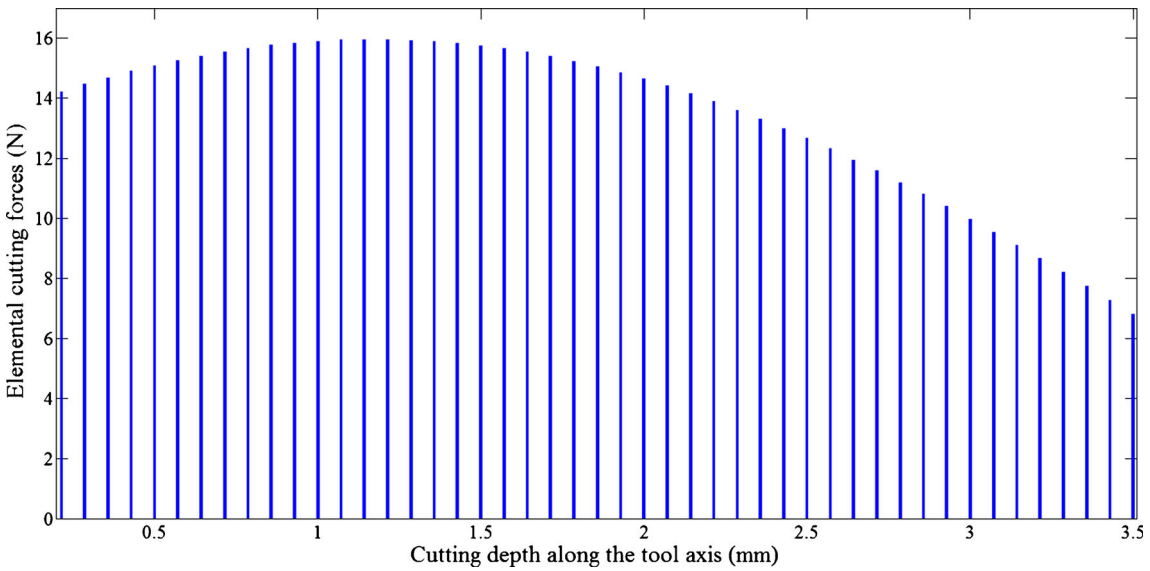

Fig. 13 Elemental cutting forces (*Fy-max*) distributed along the tool axis

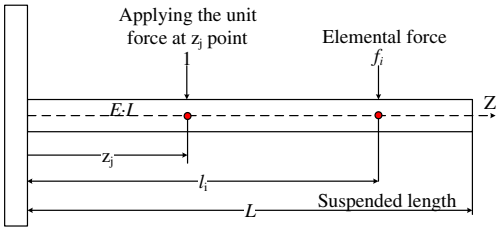

Fig. 14 Unit loading algorithm for predicting the tool deflection

experiments are carried out via FEA simulation using *AdvantEdge* which is a commercial CAE software for metal cutting shown in Fig. 10. The material properties of end mill and work-piece have been provided in the material database of *AdvantEdge* listed in Table 3. The corresponding geometrical parameters are listed in Table 2, and the various machining parameters are described in Table 4. The estimated average cutting forces are approximated from the simulation results using the least square method also shown in Table 4. According to Ref [2], the average cutting forces for full immersion milling can be expressed as following:

$$\begin{cases} \overline{F}_x = -\dfrac{Na}{4}K_{rc}c - \dfrac{Na}{\pi}K_{re} \\ \overline{F}_y = +\dfrac{Na}{4}K_{tc}c + \dfrac{Na}{\pi}K_{te} \end{cases}, \tag{11}$$

where, N is the tooth number, a is the axial cutting depth, and c is the feed rate.

As shown in Fig. 11, the linear functions are applied to fit the test data. Finally, integrating Eq. (11) and the fitting functions, the cutting coefficients can be derived and presented in Table 5.

Since the cutting coefficients have been obtained through FEA simulation, cutting forces can be predicted under any cutting condition via substituting the cutting coefficients into the force prediction program. An example is given to predict the cutting forces with a non-full-immersion case. As shown in Fig. 12, the total cutting forces within one rotation (360°) for AISI 4140 are calculated with the cutting parameters: axial cutting depth 3.5 mm, radial cutting width 2.00 mm, cutting speed 160 m/min, and feed rate 0.07 mm/tooth. Other than full-immersion cutting simulation, the engagement between cutting tool and work-piece in this example is diverse which will present different cutting forces. And it is observed that *Fy* is much larger than *Fx*, thereby tool deflection in the Y direction dominates in the milling process. Besides, the elemental cutting forces (*Fy-max*) along the tool axis are also predicted in Fig. 13, which will be used in the following tool deflection calculation.

4 Tool deflection prediction

In this work, the end mill is modeled as a cantilever beam with different cross-sections to calculate the tool deflection using the unit loading theory. According to the beam deflection superposition principle, the deflection indicated by $d(z)$ can be calibrated via summing up the effect caused by the elemental cutting forces shown as the following equation:

$$d(z) = \sum_{i=1}^{M} d_i(z), \tag{12}$$

Where, d_i called elemental deflection which caused by each elemental cutting force.

As described in Fig. 14, the elemental deflection at point z_j can be derived using energy method applying unit loading and expressed in Eq. (13):

$$d_i(z_j) = \int_0^L \frac{m \cdot M}{E \cdot I} dl, \tag{13}$$

Where m is the torque caused by the unit force and can be represented as: $m = \begin{cases} z_j - l, & l < z_j \\ 0, & l \geq z_j \end{cases}$ and M is the torque caused by the elemental force and expressed as: $M = \begin{cases} f_i \cdot (l_i - l), & l < l_i \\ 0, & l \geq l_i \end{cases}$, and I is the area moment inertia for the corresponding cross-section.

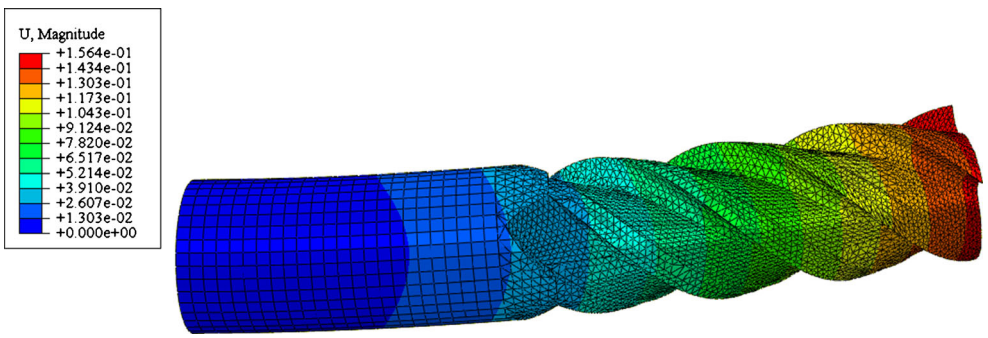

Fig. 15 Tool deflection prediction with FEA

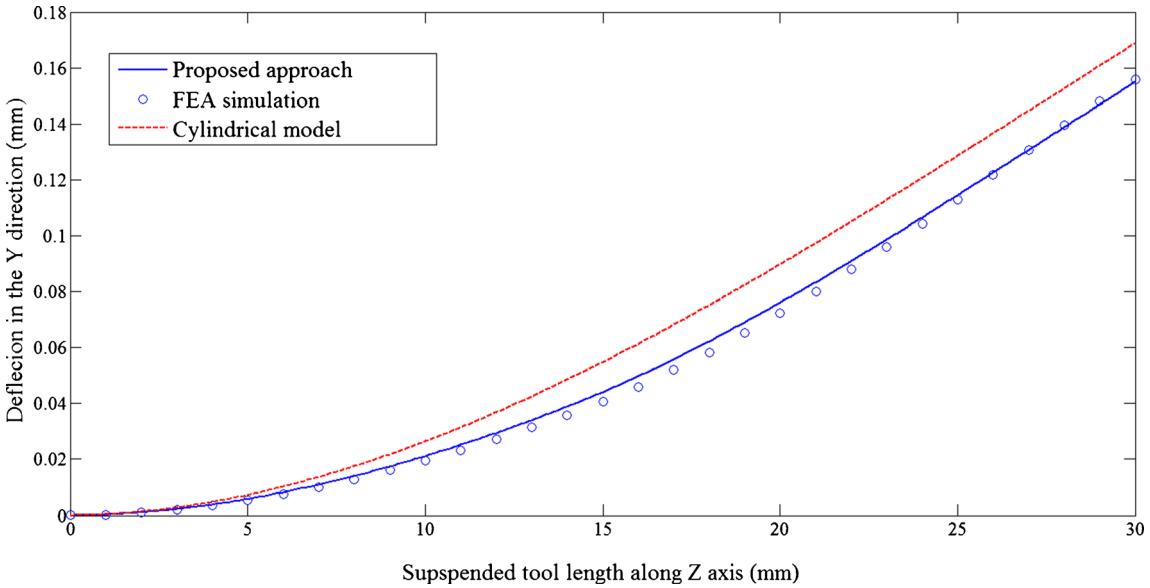

Fig. 16 Tool deflection prediction with different models

Generally, the integration formula of Eq. (13) can be calibrated through numerical method by discretizing the beam into finite segments shown in Eq. (14), which could be easily programmed using computer.

$$d_i(z_j) = \sum_{i=1}^{n} \frac{m \cdot M}{E \cdot I} \cdot \Delta l \tag{14}$$

With Eqs. (12) and (14), the deflection caused by the elemental cutting forces can be obtained at any point along the beam axis.

5 Validation and application

In this research, the developed CAD model of end mill in Fig. 6 is used to verify the proposed deflection model. The suspended tool length in this example is truncated as 30 mm, and the corresponding material properties have been described in Table 3. And also the moment of inertia of end mill is provided in Fig. 7. With all the above information, a Matlab program is developed to calculate the maximum tool defection in Y direction under elemental cutting forces *Fy-max* with the unit loading algorithm. The prediction result is shown in

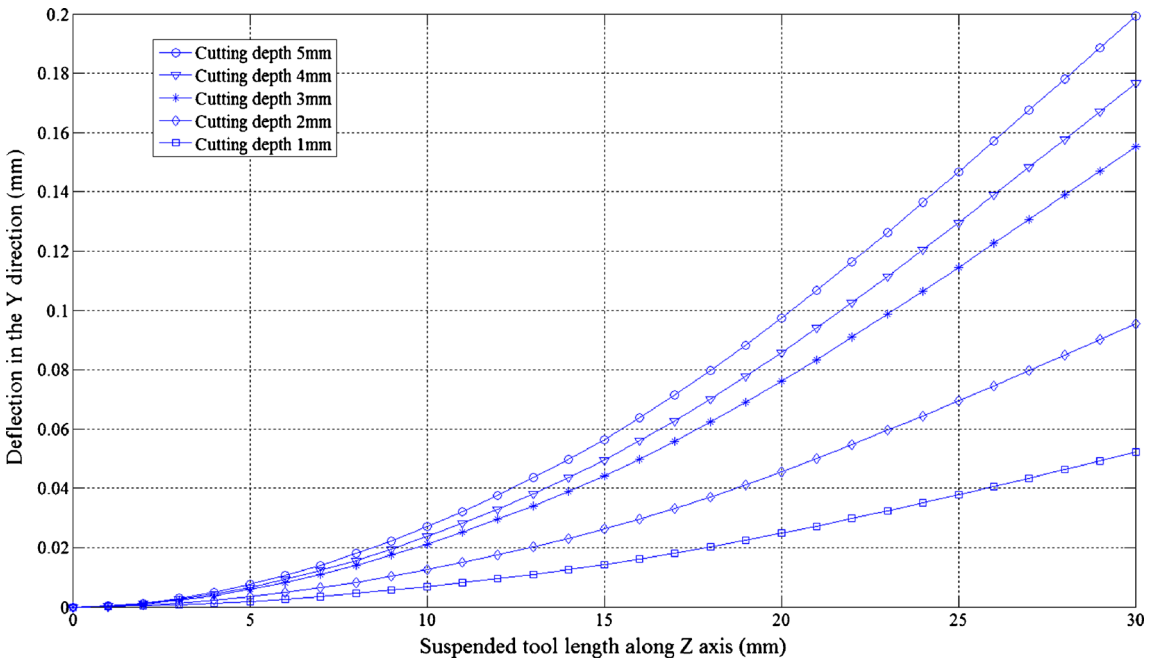

Fig. 17 Tool deflection with various cutting depth

Fig. 16. In order to evaluate the accuracy of the prediction results, a FEA simulation is conducted with the elemental cutting forces applied along the tool axis using ABAQUS shown in Fig. 15. The CAD model is partitioned into shank and flute to improve the meshing quality. And the FEA result is export with a dataset and plot in Fig. 16. The result shows a rather good agreement between the proposed analytical approach and the FEA simulation result. However, the running time for FEA (25 min) is much longer than the proposed approach (1.9 s) with the same computer. Besides, the proposed approach is also compared with the cylindrical model, which shows that the tool deflection with cylindrical model is over-predicted.

As aforementioned, the tool deflection will affect the machining efficiency and quality. A deflection diagram with various cutting depth for the developed end mill is described in Fig. 17, which can be applied to select the proper machining parameters in workshop. Furthermore, based on the proposed CAD/CAM/CAE approach, the prediction results can be fed back to improve the end mill design, such as increasing the core radius to enforce the rigidity or sharping the rake angle to reduce cutting forces.

6 Conclusions

In this paper, a parametric CAD model of end mills including the flutes and cutting edges is developed and verified via modeling its grinding processes. Using this model, a FEA cutting simulation is carried out to predict the cutting coefficients for AISI 4140 alloy steel, and then, the distribution of cutting forces is calculated. The tool defection can be accurately predicted using the unit loading algorithm integrated with the CAD model and distributed elemental cutting forces. In addition to predicting the tool deflection, the developed CAD model can be further used to improve the design of end mills via FEA simulation.

References

1. Kline WA, DeVor RE, Shareef IA (1982) The prediction of surface accuracy in end milling. ASME J Eng Ind 104(3):272–278
2. Altintas Y (2000) Manufacturing automation: metal cutting mechanics, machine tool vibrations, and CNC design. Cambridge University Press, New York
3. Shaw MC (2005) Metal cutting principles. Oxford University Press, New York
4. Boothroyd G, Knight WA (2006) Fundamentals of machining and machine tools. Taylor and Francis, Boca Raton
5. Cheng K (2009) Machining dynamics: fundamentals, applications and practice. Springer, London
6. Jiang F, Li JF, Yan L et al (2010) Optimizing end-milling parameters for surface roughness under different cooling/lubrication conditions. Int J Adv Manuf Technol 51:841–851
7. Salgado MA, Lacalle LNL, Lamikiz A, Munoa J, Sanchez JA (2005) Evaluation of the stiffness chain on the deflection of end-mills under cutting forces. Int J Mach Tools Manuf 45(6):727–739
8. Ratchev S, Liu S, Huang W, Becker AA (2007) Machining simulation and system integration combining FE analysis and cutting mechanics modelling. Int J Adv Manuf Technol 35(1–2):55–65
9. Kops L, Vo DT (1990) Determination of the equivalent diameter of an end mill based on its compliance. CIRP Ann Manuf Technol 39:93–96
10. Xu AP, Qu YX, Zhang DW, Huang T (2003) Simulation and experimental investigation of the end milling process considering the cutter flexibility. Int J Mach Tools Manuf 43:283–292
11. Lapez DL, Lamikiz A, SAnchez JA, Salgado MA (2004) Effects of tool deflection in the high-speed milling of inclined surfaces. Int J Adv Manuf Technol 24:621–631
12. Larue A, Anselmetti B (2004) A prediction of the machining defects in flank milling. Int J Adv Manuf Technol 24:102–111
13. Kim SJ (2007) Short and safe tool setting by safe space in NC machining. Int J Adv Manuf Technol 33:1017–1023
14. Kivanc EB, Budak E (2004) Structural modeling of end mills for form error and stability analysis. Int J Mach Tools Manuf 44:1151–1161
15. Chen J, Lee BY, Chen CH (2008) Planning and analysis of grinding processes for end mills of cemented tungsten carbide. J Mater Process Technol 201:618–622
16. Kaldor S, Rafael AM, Messinger D (1988) On the CAD of profiles for cutters and helical flutes—geometrical aspects. CIRP Ann Manuf Technol 37:53–56
17. Kim Y, Ko S (2002) Development of design and manufacturing technology for end mills in machining hardened steel. J Mater Process Technol 130:653–661
18. Rababah, MM, Chen, ZC, Wang, LM (2012) A new approach to five-axis CNC flute grinding of solid end-mills. ICHSM2012: 421–432
19. Kim JH, Park JW, Ko TJ (2008) End mill design and machining via cutting simulation. CAD 40:324–333